

Event-based Visual Inertial Velometer

Xiuyuan Lu^{1*}, Yi Zhou^{2*}, Shaojie Shen¹

Abstract—Neuromorphic event-based cameras are bio-inspired visual sensors with asynchronous pixels and extremely high temporal resolution. Such favorable properties make them an excellent choice for solving state estimation tasks under aggressive ego motion. However, failures of camera pose tracking are frequently witnessed in state-of-the-art event-based visual odometry systems when the local map cannot be updated in time. One of the biggest roadblocks for this specific field is the absence of efficient and robust methods for data association without imposing any assumption on the environment. This problem seems, however, unlikely to be addressed as in standard vision due to the motion-dependent observability of event data. Therefore, we propose a mapping-free design for event-based visual-inertial state estimation in this paper. Instead of estimating the position of the event camera, we find that recovering the instantaneous linear velocity is more consistent with the differential working principle of event cameras. The proposed event-based visual-inertial velometer leverages a continuous-time formulation that incrementally fuses the heterogeneous measurements from a stereo event camera and an inertial measurement unit. Experiments on the synthetic dataset demonstrate that the proposed method can recover instantaneous linear velocity in metric scale with low latency.

I. INTRODUCTION

As opposed to standard cameras that capture synchronously the absolute brightness at a fixed frame rate, event-based cameras are bio-inspired sensors that acquire visual information in the form of a stream of asynchronous per-pixel intensity changes (called “events”). Endowed with micro-second temporal resolution, event cameras can sense at exactly the same rate of the scene dynamics (induced by either ego motion or independent moving objects). Consequently, they do not suffer from motion blur and are qualified for state estimation tasks involving aggressive ego motion. The main challenge of building such an event-based visual state estimator (a.k.a event-based visual odometry) is to solve in real time the tracking and mapping sub-problems by exploiting photometric and geometric constraints encoded in the generation model of events.

Although event-based methods for camera pose tracking [1, 2] have been proved effective in tackling aggressive ego-motion estimation, most event-based VO systems are not always qualified. Early works using a monocular event-based camera (e.g., [3, 4]) require a very gentle motion (typically a local-loop behavior) for the initialization of a local 3D map,

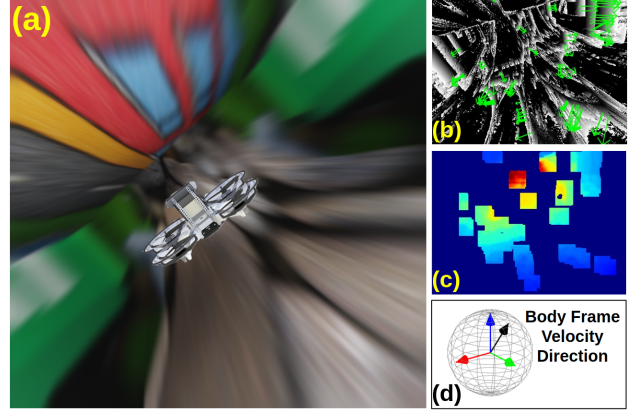


Fig. 1: The proposed system takes as input the event data from a stereo event-based camera and inertial measurements from an IMU. (a) Aggressive maneuvers of a drone through a narrow corridor. (b) Event-based normal flow estimates. (c) Corresponding depth estimates. (d) Illustration of the normalized instantaneous linear velocity estimation result.

based on which the camera pose can be tracked using a 3D-2D registration pipeline. To remove such a limitation on the initialization, Zhou *et al.* [5] further use a stereo event-based camera to improve the efficiency and accuracy of mapping. However, tracking failure is still witnessed when the ego motion of the camera suddenly becomes violent (mainly in terms of the angular velocity). This is basically due to that the mapping sub-problem solver cannot update the local map in time.

To circumvent this issue, researchers resort to visual-inertial fusion and feature-based methods. Although the event-inertial combination seems not as complimentary as the standard-visual-inertial counterpart, it is still beneficial to fuse event data with measurements of an inertial measurement unit (IMU). First, an IMU’s measurements can be used as a motion prior to propagate the estimated state. Besides, such motion prior can be leveraged to obtain a motion-compensated image of warped events (IWE), on top of which a feature-based pipeline can be simply built [6]. Obviously, the success of [6] largely relies on a sharp IWE, which is obtained via a geometric 3D-2D warping operation that requires the median depth of the local map. This warping operation, however, can easily fail if there are relatively large depth variations. To alleviate the front end’s dependence on motion prior, some works [7, 8] straightforwardly establish feature association on simple image-like representations of

¹The Department of Electronic and Computer Engineering at the Hong Kong University of Science and Technology, Hong Kong SAR, China.

²Neuromorphic Automation and Intelligence Lab (NAIL), School of Robotics, Hunan University, Changsha, Hunan, China.

*Equal contribution. Corresponding author: Xiuyuan Lu. Email: xluaaj@connect.ust.hk

events (e.g., time surfaces [9]). These ad hoc solutions may work to some extent, but the success of big-baseline feature matching is hardly guaranteed. This is due to the fact that edges parallel to the epipolar line hardly trigger any events, and thus, junction-shape patterns may not be observed completely. Consequently, the appearance similarity evaluated on such naive image-like representations could be violated in a sudden variation of linear velocity.

Noticing the dependence on the first-order kinematics, [10, 11] propose a set of speed-invariant representations, which lead to constant thickness of edge patterns irrelevant to camera speed. Though we have witnessed a lot of trials on event-based feature detection and tracking [11]–[14], most of them either cannot give satisfied feature tracking results as their standard-vision counterparts [15, 16] do, or are computationally inefficient for real-time applications. It’s also worth mentioning that few works [17]–[19] manage to establish efficiently event-to-edge association, based on which parallel tracking and mapping is achieved under aggressive motion at an ultra-frame rate. However, these solutions are only applicable in man-made structural environments. All these issues drive us to think about a question: Is there a more rational design of state estimation for an event-based visual-inertial system that is more consistent with the differential working principle of event cameras?

To answer this question, we propose a first-order kinematic state estimator, namely a velometer, using a stereo event-based camera and an IMU. Considering the special working principle of event cameras, we propose a continuous-time pipeline for the linear velocity estimation problem. Specifically, our approach exploits the generative model of event-based normal flow induced by the first-order kinematics of the event camera. Besides, the dynamic constraint from the IMU is also utilized. The contribution of this paper is summarized as follows:

- A novel design of state estimator for an event-based visual-inertial system, which exploits the differential nature of event cameras and recovers the first-order kinematic state (i.e., linear velocity) by fusing events and inertial measurements.
- A rigorous derivation for computing normal flow from spatial-temporal gradients of event data.
- A continuous-time pipeline for event-based visual-inertial fusion, which can handle asynchronous event measurements and establish data association with temporally nonaligned measurements from the accelerometer.

The rest of the paper is organized as follows. We first clarify the notion and revisit several key concepts as preliminaries in Sec. II. Our method is discussed in Sec. III, followed with the experimental evaluation in Sec. IV. Finally, the conclusion is drawn in Sec. V.

II. PROBLEM STATEMENT AND PRELIMINARIES

Let \mathcal{X}^A denote a state \mathcal{X} being described in the coordinate system A, and the state \mathcal{X} can be position \mathbf{r} , linear velocity \mathbf{v} , and angular velocity $\boldsymbol{\omega}$, etc. The relative pose between

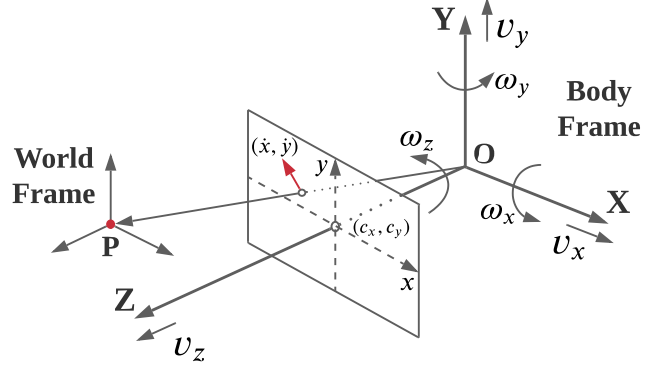


Fig. 2: Geometry and kinematics involved in the problem of motion flow. An ideal perspective camera model is used to illustrate that the 3D point \mathbf{P} is projected on the image plane. The components of both linear velocity and angular velocity are marked along their corresponding axis. The resulting motion flow is denoted by the red vector (\dot{x}, \dot{y}) .

two coordinate systems (e.g., the world frame W and the body frame B) is denoted by a rigid transformation $\mathbf{T}_{WB} \doteq \{\mathbf{R}_{WB}, \mathbf{t}_{WB}\}$, which consists of a rotation \mathbf{R}_{WB} and a translation \mathbf{t}_{WB} . Given raw output from a stereo event camera and an IMU, the goal is to estimate real-scale linear velocity \mathbf{v}^B of the sensor suite. We assume that the stereo event-based camera has been pre-calibrated, including the spatial-temporal calibration between the left and right event cameras, and between the left camera and the IMU. For simplification, we further assume that the left camera’s coordinate system coincides with that of the IMU, which is denoted as the body coordinate system or body frame (B).

To explain our method, we need to revisit several essential concepts as preliminaries, including *motion flow*, *normal flow*, and *event-based depth estimation*.

A. Motion Flow

Motion flow, also known as optical flow, refers to derivatives of a 2D image location w.r.t time. It describes how a 2D point would traverse on the image plane. As illustrated in Fig. 2, the motion flow of a textured 3D point $\mathbf{P}^B = [X, Y, Z]^T$ can be determined according to the famous equation

$$\begin{aligned} \begin{bmatrix} \dot{x}(t) \\ \dot{y}(t) \end{bmatrix} &= \begin{bmatrix} \frac{v_z x' - f v_x}{Z} + \frac{\omega_x}{f} x' y' - \omega_y (f + \frac{x'^2}{f}) + \omega_z y' \\ \frac{v_z y' - f v_y}{Z} + \omega_x (f + \frac{y'^2}{f}) - \frac{\omega_y}{f} x' y' - \omega_z x' \end{bmatrix} \\ &= \frac{1}{Z(\mathbf{x})} \mathbf{A}(\mathbf{x}) \mathbf{v}^B(t) + \mathbf{B}(\mathbf{x}) \boldsymbol{\omega}^B(t), \end{aligned} \quad (1)$$

where (\dot{x}, \dot{y}) denotes the motion flow vector at pixel $\mathbf{x} \doteq (x, y)$, $\boldsymbol{\omega}^B = [\omega_x, \omega_y, \omega_z]$ the angular velocity, $\mathbf{v}^B = [v_x, v_y, v_z]$ the linear velocity, and f the focal length. The relative image coordinates w.r.t the optical centre (c_x, c_y) are denoted by x' and y' , namely $x' \doteq x - c_x$ and $y' \doteq y - c_y$.

The motion flow equation (1) is first disclosed in [20]. It is clearly demonstrated that the motion flow is uniquely

determined by the 3D information (Z) and the first-order kinematics of the camera (\mathbf{v}^B and $\boldsymbol{\omega}^B$). In other words, given the angular velocity $\boldsymbol{\omega}^B$ (e.g., obtained from an IMU's measurements) at a time instant, the linear velocity \mathbf{v}^B can be estimated if the motion flow and depth information at *at least* two pixels are known.

B. Normal Flow

For standard vision, the motion flow is typically determined according to the *Horn-Schunck* model [21], which assumes that the brightness of a point remains constant when observed from two spatial and temporal neighbouring perspectives. By expanding the image brightness function with first-order Taylor expansion, the brightness-constancy constraint goes as,

$$I(\mathbf{x} + d\mathbf{x}, t + dt) \approx I(\mathbf{x}, t) + \nabla_{\mathbf{x}} I(\mathbf{x}) \begin{bmatrix} dx \\ dy \end{bmatrix} + \nabla_t I(\mathbf{x}) dt. \quad (2)$$

Actually, this equation provides only one constraint such that only the partial component parallel to the image gradient direction can be determined as

$$\dot{\mathbf{x}}_n(t) = -\frac{\nabla_t I(\mathbf{x})}{\|\nabla_{\mathbf{x}} I(\mathbf{x})\|^2} \nabla_{\mathbf{x}} I(\mathbf{x}), \quad (3)$$

where $\dot{\mathbf{x}}_n$ denotes the projection of the flow $\dot{\mathbf{x}}$ on the image gradient direction $\nabla_{\mathbf{x}} I$. This is referred to as the well-known *aperture problem*, and the partial component $\dot{\mathbf{x}}_n$ is typically called *normal flow*.

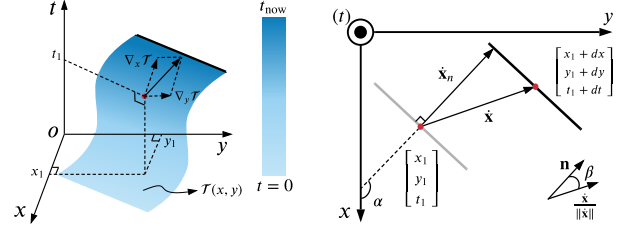
Let \mathbf{n} denote the image gradient direction at \mathbf{x} , namely $\mathbf{n} = \frac{\nabla_{\mathbf{x}} I(\mathbf{x})}{\|\nabla_{\mathbf{x}} I(\mathbf{x})\|}$. By multiplying both sides of Eq. 1 with \mathbf{n}^T , we obtain

$$\|\dot{\mathbf{x}}_n(t)\| = \frac{1}{Z(\mathbf{x})} \mathbf{n}^T \mathbf{A}(\mathbf{x})^B \mathbf{v}(t) + \mathbf{n}^T \mathbf{B}(\mathbf{x})^B \boldsymbol{\omega}(t). \quad (4)$$

Since normal flows rather than full motion flows can be estimated straightforwardly from raw events, Eq. 4 is used as a constraint in the estimation of linear velocity.

C. Event-based Depth Estimation

Existing methods of recovering depth information from event data can be classified into two categories. The first category is called the “temporal stereo” method, in which a monocular event-based camera is more often used. Temporal stereo methods assume the camera’s motion to be known as a prior [22, 23]. They utilize events occurred over a temporal window to determine the 3D location of structures by searching the maximum in the disparity space image (DSI) through either voting in the discrete space [22, 23] or in a way of continuous optimization [24]. The second category is called the “instantaneous stereo” method, which typically applies a stereo event camera that have been calibrated extrinsically and synchronized temporally [25]–[27]. Typically, this kind of methods consists of two steps: 1) Searching corresponding events occurred in the left and right event cameras; 2) Triangulation. To enhance the ratio of true-positive matching, state-of-the-art methods [5, 28, 29] utilize a hybrid metric to measure the similarity of two events, which jointly considers temporal coherence,



(a) Temporal flow estimation as spatio-temporal planar fitting. (b) Trigonometry in regard to motion flow $\dot{\mathbf{x}}$, normal flow $\dot{\mathbf{x}}_n$ and brightness gradient direction \mathbf{n} .

Fig. 3: General principles of normal flow estimation from raw event stream. (a) A time surface $\mathcal{T}(x, y)$ is spanned in the spatio-temporal domain as the edge (black) traverses. The temporal flow $\nabla_{\mathbf{x}} \mathcal{T}$ can be estimated by fitting a local plane. A color scale for the temporal values is provided aside. The darker the color, the closer the time is to the current moment. (b) The normal flow $\dot{\mathbf{x}}_n$, namely the component of the motion flow $\dot{\mathbf{x}}$ along the direction of brightness gradient \mathbf{n} , is parallel to the temporal flow $\nabla_{\mathbf{x}} \mathcal{T}$.

epipolar constraint, and motion consistency in the spatio-temporal neighborhood. Since depth estimation is not the focus of this work, we simply apply the instantaneous stereo matching method (*i.e.* block matching on time surfaces [9]) implemented in [5].

III. METHODOLOGY

Given as input the raw events from a stereo event camera and the measurements from an IMU, the goal is to recover the instantaneous linear velocity in metric scale. In this section, we first introduce our method of event-based normal flow estimation (III-A). Second, we present a continuous-time approach that fuses the two heterogeneous measurements by incrementally fitting a cubic B-spline in the space of linear velocity (III-B). Finally, we discuss our initialization method (III-C).

A. Event-based Normal Flow Estimation

To estimate visual flows from raw events, a local differential approach is proposed in [30], which fits local spatio-temporal planes on the time surface composed of co-active events. The time surface is defined specifically by the function $\mathcal{T}(x, y)$, which returns the timestamp by which the most recent event occurred at pixel $[x, y]^T$. The spatio-temporal plane’s gradient is calculated as the temporal derivative w.r.t the pixel coordinate, namely $\nabla_{\mathbf{x}} \mathcal{T} \doteq [\nabla_x \mathcal{T}, \nabla_y \mathcal{T}]^T$, which reports the timestamp difference between spatially adjacent events in the direction of x and y , respectively.

Let’s assume that the brightness gradient direction is orthogonal to edges. As shown in Fig. 3(a) and Fig. 3(b), the time surface \mathcal{T} can be regarded as a temporal profile induced by the normal flow $\dot{\mathbf{x}}_n$, and we have

$$\begin{bmatrix} \nabla_x \mathcal{T} \\ \nabla_y \mathcal{T} \end{bmatrix} = \frac{1}{\|\dot{\mathbf{x}}_n\|} \begin{bmatrix} \cos(\alpha) \\ \sin(\alpha) \end{bmatrix}. \quad (5)$$

In fact, only normal flows could be recovered from temporal derivatives due to the aperture problem (β is unknown in Fig. 3(b)), and thus, the visual flow estimated by [30] does not refer to the full motion flow $\dot{\mathbf{x}}$. The method in [30] is partially correct in the sense that the temporal gradient reveals the normal flow's direction. The reciprocal of the temporal gradient's components would not straightforwardly give correct normal flows. The amplitude of the normal flow can be determined using Eq. 5, and the normal flow vector is calculated as

$$\dot{\mathbf{x}}_n = \|\dot{\mathbf{x}}_n\| \mathbf{n} = \frac{1}{\sqrt{\nabla_x \mathcal{T}^2 + \nabla_y \mathcal{T}^2}} \mathbf{n}, \quad (6)$$

where $\mathbf{n} = \frac{\nabla_x \mathcal{T}}{\|\nabla_x \mathcal{T}\|}$ refers to the direction of the normal flow. We justify our derivation by comparing against the result of [30] in the experiment (Sec. IV-C).

B. Continuous-Time Linear Velocity Estimation

Although the computation of event-based normal flows cannot achieve the frequency as high as the streaming rate of event data (e.g. several million per second), it still can be much higher than the frame rate of a standard camera. Besides, the computation can be carried out in an asynchronous manner, and thus, the resulting event-based normal flows are typically not temporally aligned with the inertial measurements. Therefore, we employ a continuous-time formulation, which could bound the size of the optimization problem while enabling data association at any given time. Specifically, we use a cubic B-spline based parametric model to represent the continuous-time linear velocity as

$$\mathbf{v}^B(u(t)) = \sum_{i=0}^3 B_{i,3}(u(t)) \mathbf{c}_i, \quad (7)$$

where $B_{i,k}$ denotes the basis function, i the index of control points, k ($=3$) the order of the spline and $\mathbf{c}_i \in \mathbb{R}^3$ the corresponding control point defined in the space of linear velocity. The function $u(\cdot)$ is a normalization operator, which transfers time t to the spline's parameter domain by means of basis translation [31].

Our goal is to fit a cubic B-spline that satisfies jointly the following two criteria: 1) The predicted normal flows are maximally consistent with the asynchronous normal flow measurements; and 2) The first-order derivative of the spline complies maximally with the acceleration measurements. The first criterion can be simply evaluated using Eq. 4. The second criterion is evaluated, from another equivalent perspective, by calculating the difference between the predicted velocity increment and the pre-integration of acceleration in a local frame.

Let's denote the raw accelerometer and gyroscope measurements, $\tilde{\mathbf{a}}_t$ and $\tilde{\boldsymbol{\omega}}_t$, in the body frame at time t by

$$\begin{aligned} \tilde{\mathbf{a}}_t &= \mathbf{a}_t + \mathbf{b}_{a_t} + \mathbf{R}_w^t \mathbf{g}^w + \mathbf{n}_a, \\ \tilde{\boldsymbol{\omega}}_t &= \boldsymbol{\omega}_t + \mathbf{b}_{\omega_t} + \mathbf{n}_w, \end{aligned} \quad (8)$$

where \mathbf{b}_a and \mathbf{b}_ω are the accelerometer and gyroscope biases, while \mathbf{n}_a and \mathbf{n}_w the additive noise correspondingly. Let's further consider the IMU pre-integration [32] during the

time interval $[t_i, t_{i+1}]$. Assuming the IMU biases are known, we integrate the inertial measurements in the local frame \mathbf{B}_i (the body frame at time t_i) as

$$\begin{aligned} \tilde{\boldsymbol{\beta}}_{\mathbf{B}_{i+1}}^{\mathbf{B}_i} &= \int_{t_i}^{t_{i+1}} \mathbf{R}_t^{\mathbf{B}_i} (\tilde{\mathbf{a}}_t - \mathbf{b}_{a_t} - \mathbf{n}_a) dt, \\ \tilde{\boldsymbol{\gamma}}_{\mathbf{B}_{i+1}}^{\mathbf{B}_i} &= \int_{t_i}^{t_{i+1}} \frac{1}{2} \boldsymbol{\Omega}(\tilde{\boldsymbol{\omega}}_t - \mathbf{b}_{\omega_t} - \mathbf{n}_w) \boldsymbol{\gamma}_t^{\mathbf{B}_i} dt, \end{aligned} \quad (9)$$

where $\boldsymbol{\Omega}(\boldsymbol{\omega}) = \begin{bmatrix} -[\boldsymbol{\omega}]_\times & \boldsymbol{\omega} \\ \boldsymbol{\omega}^\top & 0 \end{bmatrix}$. Then the velocity and orientation can be propagated from t_i to t_{i+1} in the world frame by

$$\begin{aligned} \mathbf{v}_{\mathbf{B}_{i+1}}^w &= \mathbf{v}_{\mathbf{B}_i}^w - \mathbf{g}^w \Delta t_i + \mathbf{R}_w^{\mathbf{B}_i} \boldsymbol{\beta}_{\mathbf{B}_{i+1}}^{\mathbf{B}_i}, \\ \mathbf{q}_{\mathbf{B}_{i+1}}^w &= \mathbf{q}_{\mathbf{B}_i}^w \otimes \boldsymbol{\gamma}_{\mathbf{B}_{i+1}}^{\mathbf{B}_i}. \end{aligned} \quad (10)$$

Consequently, the predicted velocity increment during the time interval can be calculated as

$$\hat{\boldsymbol{\beta}}_{t_{i+1}}^{t_i} = \mathbf{R}(\tilde{\boldsymbol{\gamma}}_{t_{i+1}}^{t_i}) \mathbf{v}_{\mathbf{B}_{i+1}}^{\mathbf{B}_{i+1}} + \mathbf{g}^{\mathbf{B}_i} \Delta t_i - \mathbf{v}_{\mathbf{B}_i}^{\mathbf{B}_i}. \quad (11)$$

Now let's discuss the formulation of the continuous-time state estimation problem. The full state vector is defined as:

$$\begin{aligned} \mathcal{X} &= [\mathbf{c}_0, \mathbf{c}_1, \dots, \mathbf{c}_n, \mathbf{b}_0, \mathbf{b}_1, \dots, \mathbf{b}_{n-3}], \\ \mathbf{b}_k &= [\mathbf{b}_{a_k}, \mathbf{b}_{\omega_k}], k \in [0, n-3], \end{aligned} \quad (12)$$

where n denotes the total number of control points, and \mathbf{b}_k the IMU bias in the k -th B-spline segment. Note that there are $n-3$ cubic B-spline segments in the optimization. Since each segment of the B-spline is short, we simply assume the biases are constant within each segment.

Combining Eq. 4, Eq. 9 and Eq. 11, we finally create the following objective function,

$$\mathcal{X}^* = \arg \min_{\mathcal{X}} \mathcal{C}, \quad (13)$$

where the cost is defined as

$$\begin{aligned} \mathcal{C} &\doteq \sum_{t \in \mathcal{S}} \left\| \|\dot{\mathbf{x}}_n(t)\| - \frac{\mathbf{n}^\top \mathbf{A}(\mathbf{x}) \mathbf{v}^B(t)}{Z_t(\mathbf{x})} - \mathbf{n}^\top \mathbf{B}(\mathbf{x}) \boldsymbol{\omega}^B(t) \right\|_{\mathbf{P}_c}^2 \\ &+ \sum_i^M \left\| \tilde{\boldsymbol{\beta}}_{t_{i+1}}^{t_i} - \mathbf{R}(\tilde{\boldsymbol{\gamma}}_{t_{i+1}}^{t_i}) \mathbf{v}_{\mathbf{B}_{i+1}}^{\mathbf{B}_{i+1}} - \mathbf{g}^{\mathbf{B}_i} \Delta t_i + \mathbf{v}_{\mathbf{B}_i}^{\mathbf{B}_i} \right\|_{\mathbf{P}_{i+1}^i}^2 \\ &+ \sum_i^M \lambda (|\hat{\mathbf{g}}^{\mathbf{B}_i}| - c_g)^2. \end{aligned} \quad (14)$$

The first two terms implement the above-mentioned two criteria, where \mathcal{S} denotes the timestamp set of all involved normal flow estimates, and M the number of time intervals for IMU pre-integration. To obtain a maximum a posteriori estimate, we apply the Mahalanobis norm to both measurement residuals. The normal-flow covariance \mathbf{P}_c is set empirically as a fixed one. The covariance of the IMU measurements \mathbf{P}_{i+1}^i is derived from the dynamics of error terms of Eq. 9 [33]. The gravity in the body frame ($\hat{\mathbf{g}}^{\mathbf{B}_i}$) can be constantly estimated using the body-frame velocity and acceleration by

$$\hat{\mathbf{g}}^{\mathbf{B}_i} = -\dot{\mathbf{v}}_{\mathbf{B}_i}^{\mathbf{B}_i} - [\tilde{\boldsymbol{\omega}}_{t_i} - \mathbf{b}_{\omega_{t_i}}]_\times \mathbf{v}_{\mathbf{B}_i}^{\mathbf{B}_i} + \tilde{\mathbf{a}}(t_i) - \mathbf{b}_{a_{t_i}}. \quad (15)$$

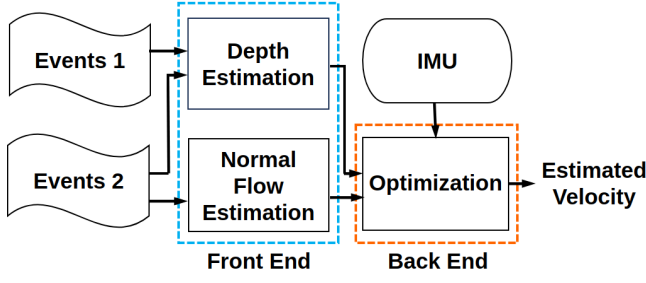


Fig. 4: Flowchart of the proposed event-based visual-inertial velometer system. The system takes as input the events from a stereo event camera and an IMU's inertial measurements, and reports the estimated linear velocity.

Since the orientation is not included in the state vector \mathcal{X} , we simply propagate the orientation with pre-integration of raw angular velocities. The third term is based on the prior information that the real gravity magnitude (c_g) is fixed and known. It minimizes the magnitude difference, and λ is a user-defined weight factor.

C. Initialization

To initialize the non-linear optimization problem (Eq. 14), we propose a linear way to coarsely determine the instantaneous linear velocity. Given as input the calculated normal flows¹, their corresponding depth information, and the corresponding measurements of instantaneous angular velocity, a linear system with linear velocity ${}^B\mathbf{v}$ as unknown can be established based on Eq 4:

$$\begin{bmatrix} \mathbf{n}_1^T \mathbf{A}_1 \\ \vdots \\ \mathbf{n}_K^T \mathbf{A}_K \end{bmatrix} {}^B\mathbf{v} = \begin{bmatrix} Z_1(\|\dot{\mathbf{x}}_{n,1}\| - \mathbf{n}_1^T \mathbf{B}_1^B \boldsymbol{\omega}) \\ \vdots \\ Z_K(\|\dot{\mathbf{x}}_{n,K}\| - \mathbf{n}_K^T \mathbf{B}_K^B \boldsymbol{\omega}) \end{bmatrix}. \quad (16)$$

A minimal solver of Eq. 16 requires three measurements, and we use RANSAC [34] for robust estimation.

IV. EXPERIMENTS

In this section, we first disclose the implementation details of our pipeline (Sec. IV-A). Second, we introduce the datasets used in the experiments (Sec. IV-B), followed with both qualitative and quantitative evaluation results and comparison against alternative solutions (Sec. IV-C). Finally, we discuss the computational performance (Sec. IV-D).

A. Implementation Details

The proposed event-based visual-inertial velometer system consists of two parts, as shown in Fig. 4. The front end implements the estimation of event-based normal flow and corresponding depth. Specifically, the event-based normal flow is computed according to Eq. 6, and the corresponding depth information is computed as mentioned in Sec. II-C. Our implementation can support either a fixed-rate computation by adaptively setting the event batch size according

¹Note that the normal flows used here are those calculated within a short time interval. In other words, their timestamps can be deemed identical.

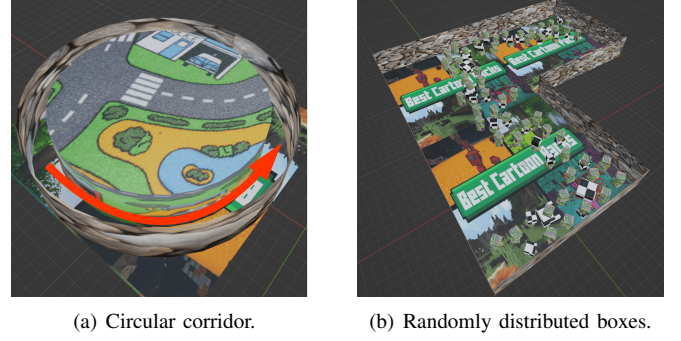


Fig. 5: Simulated scenes for synthetic data generation.

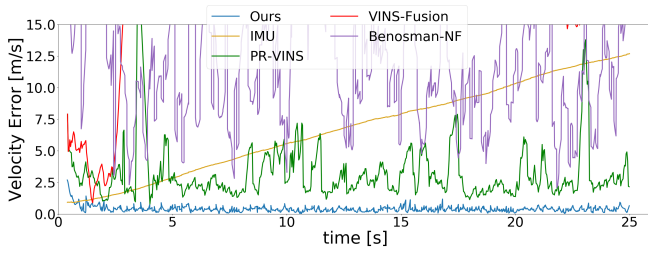
to the event rate, or a fixed-time computation that executes at a relatively high frequency. The back end implements the continuous-time nonlinear optimization pipeline using a cubic B-spline. Specifically, a uniform rational B-spline is employed, and we set the knot interval to 0.1 s. The IMU pre-integration interval is set to 0.03 s. Ceres Solver [35] is used to solve the non-linear optimization problem (Eq. 13).

B. Datasets and Evaluation Metrics

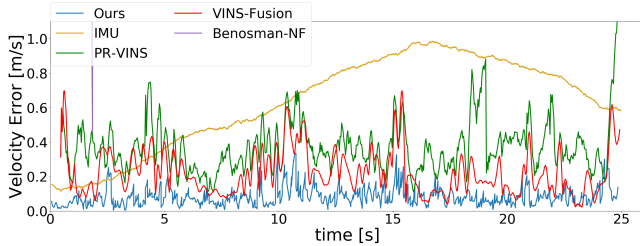
To evaluate the proposed algorithm, we generate several sequences featuring aggressive maneuvers of a drone using the ESIM simulator [36]. As shown in Fig. 5, two synthetic scenes are visualized and the corresponding kinematic characteristics of the drone are summarized in Table I. The first scene is a circular corridor in which the drone undergoes a high-speed detour. The second one features a drone traveling through randomly distributed boxes. The synthetic drone is equipped rigidly with a stereo event-based camera, a stereo standard camera and an IMU. Both of the event cameras and standard cameras share identical intrinsic parameters and extrinsic parameters, simulating a pair of the DAVIS [37] sensor. The spatial resolution of all the cameras is 346×260 pixel. Note that the standard cameras are only used by the comparative approaches in Sec. IV-C. Regarding the configuration of event generation model, the eps value is set to 0.001 and the contrast threshold is 0.5. The IMU runs at 200 Hz. The standard deviations associated to the white noise of the accelerometer and gyroscope are set to $1.86 \times 10^{-2} \text{ m/s}^2$ and $1.86 \times 10^{-3} \text{ rad/s}$, and the standard deviations of the accelerometer and gyroscope bias are set to $4.33 \times 10^{-3} \text{ m/s}^2$ and $2.66 \times 10^{-4} \text{ rad/s}$, respectively.

TABLE I: Characteristics of our synthetic datasets.

Seq. ID	Scene	Linear Vel.	Angular Vel.
1	Circular Corridor	5.68 m/s	0.66 rad/s
2	Circular Corridor	11.0 m/s	1.45 rad/s
3	Circular Corridor	18.9 m/s	2.50 rad/s
4	Randomly Distributed Boxes	2.77 m/s	2.05 rad/s
5	Randomly Distributed Boxes	3.19 m/s	3.11 rad/s



(a) Absolute velocity estimation error of Seq. 3



(b) Absolute velocity estimation error of Seq. 5.

Fig. 6: *Representative AVE results.* Note that the AVE of VINS-Fusion in (a) and the AVE of Benosman-NF in (b) are too large to be visualized inside the plot.

TABLE II: AVE of each data sequence (m/s).

Seq. ID	IMU	VINS-Fusion	PR-VINS	Benosman-NF	Ours
1	2.67	0.48	1.31	6.93	0.13
2	5.73	0.87	1.33	13.97	0.24
3	7.83	19.80	2.99	12.04	0.49
4	0.54	0.14	0.27	7.39	0.05
5	0.63	0.23	0.37	7.55	0.07

C. Evaluation Result

To demonstrate the effectiveness of our method, we compare it against several alternative solutions that can determine the linear velocity. The first one is the IMU integration, which requires only the initial orientation and linear velocity as a prior. The second one is the VINS-Fusion pipeline, which is widely applied in state estimation tasks of small unmanned aerial vehicles. To make a fair comparison, the VINS-Fusion pipeline is evaluated after being successfully initialized. Additionally, we add another two comparative methods by applying some modifications to VINS-Fusion and our pipeline. The third one is a periodically re-initialized VINS-Fusion (PR-VINS) pipeline, which is to alleviate the unfairness caused by the lost camera tracking in the original VINS-Fusion. The last one replaces the method for computing event-based normal flow in our pipeline with Benosmans' method [30] (Benosman-NF).

To quantitatively evaluate the results, we apply as evaluation metrics the Absolute Velocity Error (AVE) and Relative Velocity Error (RVE). The latter one is defined as the ratio of the AVE and the magnitude of groundtruth velocity, namely

$$\text{RVE} = \frac{|\mathbf{v}_{gt} - \mathbf{v}_{est}|}{|\mathbf{v}_{gt}|} \times 100\%. \quad (17)$$

To have a close-up view of each method's performance,

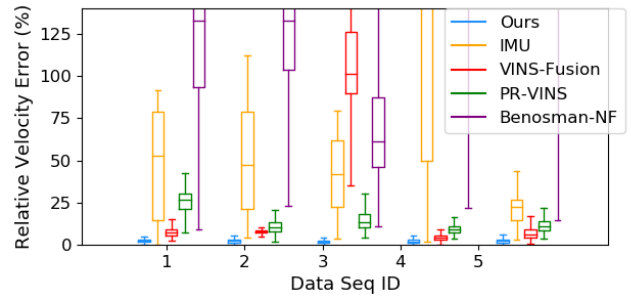


Fig. 7: Relative velocity estimation error evaluation result

TABLE III: Computation time of our algorithm

Module	Normal Flow & Depth Est.	Back-end Optimization	Overall
Avg. Time (ms)	13	10	23

we select as representatives the results of two sequences that feature the most aggressive maneuvers in each scene. As illustrated in Fig. 6, obvious accumulated errors are witnessed in the velocity estimates from the IMU-integration method. VINS-Fusion performs normally good in Seq. 5 but fails in Seq. 3 due to a failure of camera tracking caused by image blur. The AVE of PR-VINS is typically bounded to some extent, but it is still less accurate than our method. Finally, Benosman-NF typically gives bad results, which, from another perspective, justifies our derivation of event-based normal flow computation.

More detailed AVE results can be found in Table. II Correspondingly, the RVE results are illustrated using box plots in Fig. 7. As a conclusion, our method always achieves the best performance in terms of AVE and RVE.

D. Computational Performance

Our pipeline is implemented in C++ on ROS and all experiments are performed in real time on a desktop PC with an Intel Core i3700K CPU. The computation time of the main modules is summarized in Table. III. The normal flow and depth estimations are performed simultaneously in two independent threads. Fed with the front-end results, the back end ultimately solves the state estimation problem in another separated thread. The whole system can output the body-frame linear velocity up to 75 Hz.

V. CONCLUSION

We present a novel strategy for fusing event data and inertial measurements in state estimation tasks involving aggressive maneuvers. The proposed event-based visual-inertial velometer system is built on top of a continuous-time state estimation framework, which can handle data association across heterogeneous and temporally non-aligned measurements. Experiments demonstrate the effectiveness of our method, and we hope our work inspires future research in event-based state estimation.

REFERENCES

- [1] G. Gallego, J. E. Lund, E. Mueggler, H. Rebecq, T. Delbruck, and D. Scaramuzza, "Event-based, 6-dof camera tracking from photometric depth maps," *IEEE Trans. Pattern Anal. Mach. Intell.*, vol. 40, no. 10, pp. 2402–2412, 2017.
- [2] S. Bryner, G. Gallego, H. Rebecq, and D. Scaramuzza, "Event-based, direct camera tracking from a photometric 3d map using nonlinear optimization," in *2019 International Conference on Robotics and Automation (ICRA)*. IEEE, 2019, pp. 325–331.
- [3] H. Kim, S. Leutenegger, and A. J. Davison, "Real-time 3D reconstruction and 6-DoF tracking with an event camera," in *Eur. Conf. Comput. Vis. (ECCV)*, 2016, pp. 349–364.
- [4] H. Rebecq, T. Horstschäfer, G. Gallego, and D. Scaramuzza, "EVO: A geometric approach to event-based 6-DOF parallel tracking and mapping in real-time," *IEEE Robot. Autom. Lett.*, vol. 2, no. 2, pp. 593–600, 2017.
- [5] Y. Zhou, G. Gallego, and S. Shen, "Event-based stereo visual odometry," *IEEE Transactions on Robotics*, vol. 37, no. 5, pp. 1433–1450, 2021.
- [6] H. Rebecq, T. Horstschäfer, and D. Scaramuzza, "Real-time visual-inertial odometry for event cameras using keyframe-based nonlinear optimization," in *British Mach. Vis. Conf. (BMVC)*, 2017.
- [7] A. Hadviger, I. Cvišić, I. Marković, S. Vražić, and I. Petrović, "Feature-based event stereo visual odometry," in *2021 European Conference on Mobile Robots (ECMR)*. IEEE, 2021, pp. 1–6.
- [8] P. Chen, W. Guan, and P. Lu, "Esvio: Event-based stereo visual inertial odometry," *IEEE Robotics and Automation Letters*, 2023.
- [9] X. Lagorce, G. Orchard, F. Gallupi, B. E. Shi, and R. Benosman, "HOTS: A hierarchy of event-based time-surfaces for pattern recognition," *IEEE Trans. Pattern Anal. Mach. Intell.*, vol. 39, no. 7, pp. 1346–1359, July 2017.
- [10] J. Manderscheid, A. Sironi, N. Bourdis, D. Migliore, and V. Lepetit, "Speed invariant time surface for learning to detect corner points with event-based cameras," in *IEEE Conf. Comput. Vis. Pattern Recog. (CVPR)*, 2019.
- [11] A. Glover, A. Dinale, L. D. S. Rosa, S. Bamford, and C. Bartolozzi, "lutharis: A practical corner detector for event-cameras," *arXiv preprint arXiv:2105.11443*, 2021.
- [12] I. Alzugaray and M. Chli, "Asynchronous corner detection and tracking for event cameras in real-time," *IEEE Robot. Autom. Lett.*, vol. 3, no. 4, pp. 3177–3184, Oct. 2018.
- [13] —, "ACE: An efficient asynchronous corner tracker for event cameras," in *3D Vision (3DV)*, 2018, pp. 653–661.
- [14] L. Dardelet, R. Benosman, and S.-H. Ieng, "An event-by-event feature detection and tracking invariant to motion direction and velocity," *TechRxiv*, 2021. [Online]. Available: <https://doi.org/10.36227/techrxiv.17013824.v1>
- [15] E. Rublee, V. Rabaud, K. Konolige, and G. Bradski, "Orb: An efficient alternative to sift or surf," in *Int. Conf. Comput. Vis. (ICCV)*. IEEE, 2011, pp. 2564–2571.
- [16] S. Leutenegger, M. Chli, and R. Y. Siegwart, "Brisk: Binary robust invariant scalable keypoints," in *Int. Conf. Comput. Vis. (ICCV)*. IEEE, 2011, pp. 2548–2555.
- [17] W. O. Chamorro Hernandez, J. Andrade-Cetto, and J. Solà Ortega, "High-speed event camera tracking," in *British Mach. Vis. Conf. (BMVC)*, 2020.
- [18] W. Chamorro, J. Solà, and J. Andrade-Cetto, "Event-based line slam in real-time," *IEEE Robotics and Automation Letters*, vol. 7, no. 3, pp. 8146–8153, 2022.
- [19] —, "Event-imu fusion strategies for faster-than-imu estimation throughput," in *Proceedings of the IEEE/CVF Conference on Computer Vision and Pattern Recognition (CVPR) Workshops*, June 2023, pp. 3975–3982.
- [20] H. C. Longuet-Higgins and K. Prazdny, "The interpretation of a moving retinal image," *Proceedings of the Royal Society of London. Series B. Biological Sciences*, vol. 208, no. 1173, pp. 385–397, 1980.
- [21] B. K. Horn and B. G. Schunck, "Determining optical flow," *Artificial intelligence*, vol. 17, no. 1-3, pp. 185–203, 1981.
- [22] H. Rebecq, G. Gallego, and D. Scaramuzza, "EMVS: Event-based multi-view stereo," in *British Mach. Vis. Conf. (BMVC)*, 2016.
- [23] H. Rebecq, G. Gallego, E. Mueggler, and D. Scaramuzza, "EMVS: Event-based multi-view stereo—3D reconstruction with an event camera in real-time," *Int. J. Comput. Vis.*, vol. 126, no. 12, pp. 1394–1414, Dec. 2018.
- [24] G. Gallego, H. Rebecq, and D. Scaramuzza, "A unifying contrast maximization framework for event cameras, with applications to motion, depth, and optical flow estimation," in *IEEE Conf. Comput. Vis. Pattern Recog. (CVPR)*, 2018, pp. 3867–3876.
- [25] J. Kogler, M. Humenberger, and C. Sulzbachner, "Event-based stereo matching approaches for frameless address event stereo data," in *Int. Symp. Adv. Vis. Comput. (ISVC)*, 2011, pp. 674–685.
- [26] P. Rogister, R. Benosman, S.-H. Ieng, P. Lichtsteiner, and T. Delbruck, "Asynchronous event-based binocular stereo matching," *IEEE Trans. Neural Netw. Learn. Syst.*, vol. 23, no. 2, pp. 347–353, 2012.
- [27] L. A. Camunas-Mesa, T. Serrano-Gotarredona, S. H. Ieng, R. B. Benosman, and B. Linares-Barranco, "On the use of orientation filters for 3D reconstruction in event-driven stereo vision," *Front. Neurosci.*, vol. 8, p. 48, 2014.
- [28] S.-H. Ieng, J. Carneiro, M. Osswald, and R. Benosman, "Neuromorphic event-based generalized time-based stereovision," *Front. Neurosci.*, vol. 12, p. 442, 2018.
- [29] Y. Zhou, G. Gallego, H. Rebecq, L. Kneip, H. Li, and D. Scaramuzza, "Semi-dense 3D reconstruction with a stereo event camera," in *Eur. Conf. Comput. Vis. (ECCV)*, 2018, pp. 242–258.
- [30] R. Benosman, C. Clercq, X. Lagorce, S.-H. Ieng, and C. Bartolozzi, "Event-based visual flow," *IEEE Trans. Neural Netw. Learn. Syst.*, vol. 25, no. 2, pp. 407–417, 2014.
- [31] C. De Boor, "On calculating with b-splines," *Journal of Approximation theory*, vol. 6, no. 1, pp. 50–62, 1972.
- [32] C. Forster, L. Carlone, F. Dellaert, and D. Scaramuzza, "IMU preintegration on manifold for efficient visual-inertial maximum-a-posteriori estimation," in *Robotics: Science and Systems (RSS)*, 2015.
- [33] T. Qin, P. Li, and S. Shen, "VINS-Mono: A robust and versatile monocular visual-inertial state estimator," *IEEE Trans. Robot.*, vol. 34, no. 4, pp. 1004–1020, 2018.
- [34] M. A. Fischler and R. C. Bolles, "Random sample consensus: a paradigm for model fitting with applications to image analysis and automated cartography," *Commun. ACM*, vol. 24, no. 6, pp. 381–395, 1981.
- [35] A. Agarwal, K. Mierle, and Others, "Ceres solver," <http://ceres-solver.org>.
- [36] H. Rebecq, D. Gehrig, and D. Scaramuzza, "ESIM: an open event camera simulator," in *Conf. on Robotics Learning (CoRL)*, 2018.
- [37] C. Brandli, R. Berner, M. Yang, S.-C. Liu, and T. Delbruck, "A 240x180 130dB 3 μ s latency global shutter spatiotemporal vision sensor," *IEEE J. Solid-State Circuits*, vol. 49, no. 10, pp. 2333–2341, 2014.